UDC 621.3.013 https://doi.org/10.20998/2074-272X.2025.6.06

B.I. Kuznetsov, T.B. Nikitina, I.V. Bovdui, K.V. Chunikhin, V.V. Kolomiets, B.B. Kobylianskyi

Synthesis of combined shielding system for overhead power lines magnetic field normalization in residential building space

Problem. *Most studies of power frequency magnetic field reduced to safe level in residential buildings located near overhead power lines carried out based on two-dimensional magnetic field modeling, which does not allow studying of original magnetic field shielding effectiveness in residential building edges. The* ***goal*** *of the work is synthesis of combined active and multi-circuit passive shielding system to improve shielding efficiency of initial magnetic field to sanitary standards level in residential building edges generated by overhead power lines.* ***Methodology****. System synthesis methodology based on vector game solution, in which vector payoff calculated based on of Maxwell's equations solution in a quasi-stationary approximation using the COMSOL Multiphysics software. Vector game solution calculated based on hybrid optimization algorithm, which globally explores synthesis search space using Particle Swarm Optimization and gradient-based Sequential Quadratic Programming to rapidly calculated optimum synthesis point from Pareto optimal solutions taking into account binary preference relations.* ***Results.*** *During combined active and multi-circuit passive shielding system synthesisspatial arrangement coordinates of 16 contours of passive shield and two compensating windings, as well as windings currents and phases of active shield calculated. New scientific results are theoretical and experimental studies of synthesized combined active and multi-circuit passive shielding system efficiency for magnetic field created by overhead power lines.* ***Scientific novelty****. For the first time synthesis methodology for combined active and multi-circuit passive shielding system taking into account original field shielding effectiveness decrease in residential building edges for more effective reduction of industrial frequency magnetic field created by overhead power lines developed.* ***Practical value****. Practical recommendations for the reasonable choice of the spatial arrangement of a multi-circuit passive shield and two shielding windings of active shielding system for magnetic field created by overhead power lines are given. The possibility of reducing the initial magnetic field induction to the sanitary standards level is shown.* References 42, figures 16.
Key words: **overhead power line, magnetic field, combined electromagnetic active and passive shielding system, synthesis computer simulation, experimental research.**

Проблема*. Більшість досліджень з зниження рівня магнітного поля промислової частоти в житлових будинках, що розташовані поблизу повітряних ліній електропередачі, до безпечного рівня, виконані на основі двовимірного моделювання магнітного поля, що не дозволяє вивчати ефективність екранування вихідного магнітного поля на краях житлових будинків.* ***Метою*** *роботи є синтез комбінованої активної та багатоконтурної пасивної електромагнітної екрануючої систем для підвищення ефективності екранування вихідного магнітного поля до рівня санітарних норм на краях житлових будинків, що генерується повітряними лініями електропередачі.* ***Методологія****. Методологія синтезу системи заснована на рішенні векторної гри, в якій векторний виграш розраховується на основі розв'язку рівнянь Максвелла в квазістаціонарному наближенні за допомогою програмного пакету COMSOL Multiphysics. Рішення векторної гри обчислюється на основі гібридного алгоритму оптимізації, яке глобально досліджує простір пошуку для синтезу за допомогою оптимізації роєм частинок та градієнтного послідовного квадратичного програмування для швидкого обчислення оптимальної точки синтезу з системи Парето оптимальних рішень з урахуванням бінарних відношень переваг.* ***Результати****. В процесі синтезу активної та багатоконтурної пасивної електромагнітної екрануючих систем розраховано координати просторового розташування 16 контурів пасивного екрану та двох компенсаційних обмоток системи активного екранування, а також струм та фази компенсуючих обмоток системи активного екранування. Новими науковими результатами є теоретичні та експериментальні дослідження ефективності синтезованої комбінованої активної та багатоконтурної пасивної електромагнітних екрануючих систем магнітного поля, що створюється повітряними лініями електропередачі.* ***Наукова новизна****. Вперше запропонована методологія синтезу комбінованих активних та багатоконтурних пасивних електромагнітних екрануючих систем з урахуванням ефективності екранування вихідного поля на краях житлових будинків з метою більш ефективного зниження магнітного поля промислової частоти, що генерується повітряними лініями електропередачі.* ***Практична значимість****. Надано практичні рекомендації щодо обґрунтованого вибору просторового розташування багатоконтурного пасивного екрана та двох екрануючих обмоток системи активного екранування магнітного поля, що генерується повітряними лініями електропередачі. Показана можливість зниження індукції вихідного магнітного поля до рівня санітарних норм*. Бібл. 42, рис. 16.
Ключові слова: **повітряна лінія електропередачі, магнітне поле, система комбінованого електромагнітного активного та пасивного екранування, синтез комп'ютерного моделювання, експериментальне дослідження.**

Introduction. Protecting public health problem solving from electric power man-made electromagnetic field biological impact has high social significance and is extremely relevant and important task in population quality and life expectancy improving [1–3]. Reducing problem humanity priority of man-made electromagnetic fields influence has been confirmed by World Health Organization (WHO) and electromagnetic field influence on human body. A significant place in these studies occupied industrial-frequency electromagnetic field created by power transmission lines. High-voltage overhead power lines located in residential areas are industrial-frequency magnetic fields main sources, which negatively affects on population in residential buildings located along power line routes [4–7]. The basis for substantiating these conclusions was identification of carcinogenic properties of industrial-frequency magnetic field exposure with its weak but long-term effects on humans [1–3] and the development of recommendations for maximum possible reduction in magnetic fields induction level in residential areas located near power lines homes, to reduce likelihood of population cancer.

Carcinogenic properties identification and weak magnetic field action deadly danger with less than 1 μT induction during its long-term exposure to people has led to gradual introduction for magnetic field induction level strict sanitary standards and these standards constant tightening of 50–60 Hz frequency magnetic field induction boundary levels with up to WHO recommended level 0.2–0.6 μT [1–3].

Many residential buildings located in close proximity to high-voltage power lines, so that magnetic field induction level inside these buildings significantly exceeds modern sanitary standards.

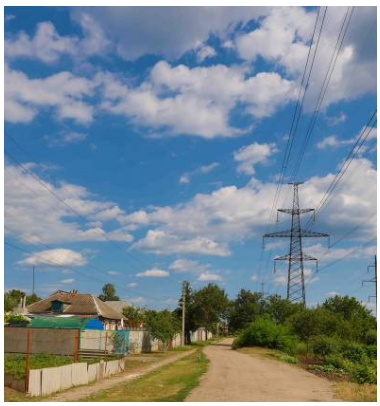

Fig. 1. Residential buildings located close to power line

For example, as shown in Fig. 1, residential buildings located in close proximity to main two-circuit power line 330 kV with split wires of 2 kA in each circuit. Next to this power line there is another double-circuit power line 110 kV 500 A of an older construction.

Numerous theoretical and experimental studies show [7–10] that the maximum permissible magnetic field level induction (0.5 μT) can be exceeded by order of magnitude or more, which poses threat to health of hundreds of thousands of citizens living closer than 100 m from overhead power lines.

In addition, due to land plots price constant rise for development, the construction of residential, administrative and other public buildings and structures in places where existing high-voltage power lines pass through continues. This condition is typical for many leading countries of the world – the USA, Israel, Italy, Spain and many others and requires the adoption of urgent measures to reduce existing power lines magnetic field level by 3-5 times [4–7]. Therefore, in many leading countries of the world, methods and means of normalizing magnetic field in energy infrastructure, public buildings, and residential buildings are being intensively developed, and these means are being widely introduced [8–12].

Most effective technology is power lines reconstruction by moving them to safe distance from residential buildings, or replacing overhead power lines with cable line. However, such reconstruction requires enormous financial resources.

Existing power lines magnetic field shielding methods are less expensive. Active contour magnetic field shielding methods provided necessary efficiency. Currently, research is being intensively carried out all over the world and various systems for active shielding of man-made magnetic field of industrial frequency are being implemented [13–18].

Overhead power lines with phase wires «triangular» arrangement often pass in close proximity to older residential buildings. This power lines are one of most dangerous wire layout options for magnetic field sources. Overhead power lines with phase wires «triangular» arrangement created magnetic field with circle shape spatio-temporal characteristic. For effective active shielding of magnetic field with such a space-time characteristic, at least two compensation windings are required for active shielding system.

Active shielding requires external power sources used to generate compensating windings appropriate magnitude and phase currents to create compensating magnetic field directed opposite to power line original magnetic field, which is necessary to desired shielding effect implement.

Active shielding systems are capable of providing power lines initial magnetic field strong weakening [4]. However, this requires a rather complex automatic control system, in which, in addition to magnetic field sensors, it is necessary to install expensive high-power equipment, such as power supplies, power converters and control system that forms the currents supplied to compensating windings to achieve of original magnetic field required suppression. Active shielding systems are significantly more expensive to develop than passive methods [13–18].

Original magnetic field with passive shielding weakening achieved by compensating field generating according to Faraday law passive shield using. Multi-circuit passive shields often used to increase initial magnetic field shielding efficiency [8]. However, passive shields have significantly lower shielding coefficient than active shields, so passive shields are often used as an addition to active shielding systems, so that hybrid active-passive shields simultaneously use both an active shielding system and passive shields of various designs [19].

In addition to solid electromagnetic shields [16], multi-circuit passive shields also used as a passive screen [20].

The diagram of such combined electromagnetic active multi-circuit passive shielding system with multi-circuit passive shields shown in Fig. 2.

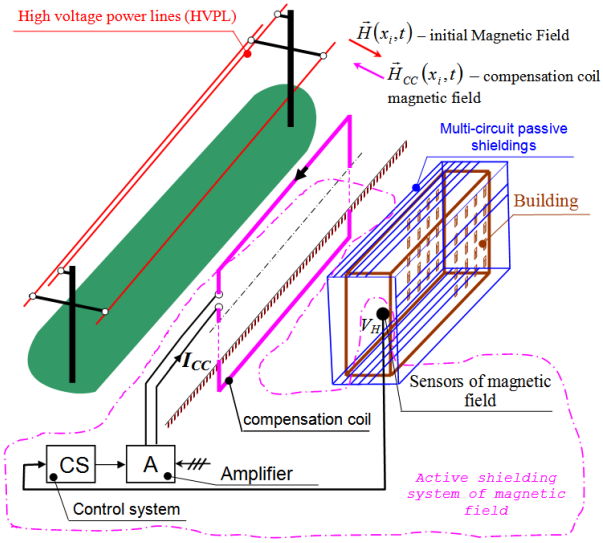

Fig. 2. Combined electromagnetic active and multi-circuit passive shielding system diagram

The active shielding system is a closed dynamic automatic control system with feedback. Using a magnetic field sensor installed in the shielding space, the resulting magnetic field measured to implement feedback.

The active shielding system generated a compensating magnetic field directed opposite to the original magnetic field using a compensating winding. The active shielding system also contains a control system and an amplifier.

With the help of a multi-circuit passive shielding system a magnetic field is generated opposite to the initial magnetic field according to the Faraday law. In this case, the initial magnetic field for the multi-circuit passive shielding system generated by power transmission line wires and compensating windings of the active shielding system.

Magnetic field induction level in residential buildings necessary reduced to safe level in apartments located at buildings edges. Most studies carried out based on two-dimensional magnetic field modeling, which does not allow studying effectiveness decrease of original field shielding in residential building edges [21–23]. Therefore, to effectively

shielding the original magnetic field throughout the entire space of a residential building, it is necessary to use a three-dimensional model of the magnetic field.

The goal of the work is synthesis of combined active and multi-circuit passive shielding system to improve shielding efficiency of initial magnetic field to sanitary standards level in residential building edges generated by overhead power lines.

Definition of geometric forward magneto static problem for passive electromagnetic multi-circuit shield. Using a system of hybrid active and multi-loop passive shielding, it is necessary to generate such a compensating magnetic field in the entire shielding space that the vector of the instantaneous value of the induction of this compensating magnetic field is directed opposite to the vector of the instantaneous value of the induction of the original magnetic field generated by the power transmission line in residential building space.

To synthesize a combined active and multi-circuit passive shielding system, it is first necessary to solve three geometric direct problems of magnetostatics for three-dimensional overhead power lines magnetic field model. The first geometric direct problem of magnetostatics calculated the vector of the instantaneous value of the induction of the initial magnetic field generated by the power transmission line at a given point of the entire screening space.

The second geometric direct problem calculated the vector of the instantaneous value of the induction of the compensating magnetic field generated by the compensating windings of the active shielding system at a given point of the entire shielding space.

The third geometric direct problem of magnetostatics calculated the vector of the instantaneous value of the induction of the compensating magnetic field generated by the compensating windings of the multi-circuit passive shielding system at a given point of the entire shielding space.

Based on the solution of these three geometric direct magnetostatic problems, a geometric inverse magnetostatic problem formulated and solved for the synthesis of a hybrid active and multi-loop passive shield. This geometric inverse magnetostatic problem is an ill-posed mathematical problem and usually formulated in the form of an optimization problem. The components of the vector objective function of this optimization problem are the effective values of the resulting magnetic field induction at the points of the entire shielding space.

As result of solving this geometric inverse problem of magnetostatics, the coordinates of the «geometric» arrangement of the compensation windings of the active and multi-circuit passive shielding system, as well as the values of currents and phases in the compensation windings of the active shielding system calculated.

Three-dimensional mathematical modeling of electromagnetic field in general case comes down to boundary value problem solving for Maxwell partial differential equations system [7].

$$rot\ \boldsymbol{H} = \boldsymbol{j} + \partial_t \boldsymbol{D} + \boldsymbol{j}_{ex}; \quad (1)$$

$$rot\ \boldsymbol{E} = -\partial_t \boldsymbol{B}, \quad (2)$$

where $\boldsymbol{E}$ – electric field strength; $\boldsymbol{H}$ – magnetic field strength; $\boldsymbol{D}$, $\boldsymbol{B}$ – electric and magnetic induction vectors; $\boldsymbol{j}$ – conduction current density; $\boldsymbol{j}_{ex}$ – density of external currents created by sources outside the region under consideration.

First equation (1) is generalized Ampere law – the total current density is magnetic field strength vortex. Second equation (2) is Faraday law differential formulation that magnetic induction change over time generates vortex electric field.

Intermediate position between constant field and rapidly changing field occupied by quasi-stationary field – electromagnetic field in which displacement currents neglected in comparison with conduction currents. Maxwell equations for quasi-stationary field have form

$$rot\ \boldsymbol{H} = \boldsymbol{j} + \boldsymbol{j}_{ex}; \quad (3)$$

$$rot\ \boldsymbol{E} = -\partial_t \boldsymbol{B}. \quad (4)$$

From (3) follows that quasi-stationary magnetic field at any given time moment completely determined by electric currents distribution at the same time moment and founded from this distribution in exactly same way as is done in magnetostatics.

Power lines magnetic field calculated based on Biot-Savart law for elementary current

$$d\boldsymbol{H}(t) = \frac{\boldsymbol{I}(t)}{4\pi \boldsymbol{R}^3}(\mathrm{d}\boldsymbol{l} \times \boldsymbol{R}), \quad (5)$$

where $\boldsymbol{R}$ – vector directed from elementary segment; d$\boldsymbol{l}$ with total current $\boldsymbol{I}(t)$ to observation point Q. Total field strength vector calculated as:

$$\boldsymbol{H}(Q,t) = \frac{\boldsymbol{I}(t)}{4\pi}\int_L \frac{(\mathrm{d}\boldsymbol{l} \times \boldsymbol{R})}{\boldsymbol{R}^3}. \quad (6)$$

This formula (6) widely used to calculate overhead power lines magnetic field instead of Maxwell equations system (3)–(4). Thus magnetic field induction dependence on current and described by (6).

Magnetic field quasi-stationary model varies with time according to sinusoidal law calculated as

$$\boldsymbol{H}(Q,t) = \boldsymbol{A}(Q)\exp j(\omega t), \quad (7)$$

where $\boldsymbol{A}(Q)$ – magnetic field strength amplitude.

Consider design of magnetic field mathematical model created by a multi-circuit passive shield, which is hybrid active-passive shield part [19]. In works [13–15] passive shield parameters considered given. These parameters calculated during active-passive shielding system design. Therefore, in contrast to works [13–15], we set initial values vector $\boldsymbol{X}_p$ of geometric dimensions, thickness and material of multi-circuit passive shield.

In works [12–15] power line currents parameters (8) considered known and do not change over time. However, power line currents magnitudes have daily, weekly and seasonal changes. Therefore, unlike works [12–15], we introduce of of the initial uncertainties parameters vector $\boldsymbol{\delta}$ of hybrid active-passive shielding system designing problem with power line wires currents and phases values uncertainties components, as well as other uncertainty parameters of electromagnetic hybrid active-passive screen, which, firstly, are initially known inaccurately, and, secondly, can changed during system operation [24–28].

Then, for given induction vector $\boldsymbol{B}_{Ra}(Q_i,\boldsymbol{X}_a,\boldsymbol{\delta},t)$ of resulting magnetic field, created by power line and only windings of active part of hybrid active-passive shield, as well as of geometric dimensions vector values $\boldsymbol{X}_p$ of multi-circuit passive contour shield, magnetic flux $\boldsymbol{\Phi}_l(\boldsymbol{X}_a,\boldsymbol{X}_p,\boldsymbol{\delta},t)$ piercing contour l of multi-circuit passive shield calculated

$$\boldsymbol{\Phi}_l(\boldsymbol{X}_a,\boldsymbol{X}_p,\boldsymbol{\delta},t) = \int_S \boldsymbol{B}_{Ra}(\boldsymbol{X}_a,\boldsymbol{\delta},t)\mathrm{d}S. \quad (8)$$

Current $\boldsymbol{I}_{Pl}(\boldsymbol{X}_a,\boldsymbol{X}_p,\boldsymbol{\delta},t)$ in complex form, induced in circuit l of multi-circuit passive shield calculated according to Ohm law and in integral form of Faraday law [9]:

$$\boldsymbol{I}_{Pl}\left(\boldsymbol{X}_a,\boldsymbol{X}_p,\boldsymbol{\delta},t\right)=-j\omega\boldsymbol{\Phi}(\boldsymbol{X}_a,\boldsymbol{X}_p,\boldsymbol{\delta},t)/\ldots \\ \ldots/(\boldsymbol{R}_l(\boldsymbol{X}_p)+j\omega\boldsymbol{L}_l(\boldsymbol{X}_p), \quad (9)$$

where $\boldsymbol{R}_l(\boldsymbol{X}_p)$ – active resistance and inductance $\boldsymbol{L}_l(\boldsymbol{X}_p)$ of circuit l of multi-circuit passive shield calculated for passive shield geometric dimensions vector values $\boldsymbol{X}_p$.

Then, for calculated values currents $\boldsymbol{I}_{Pl}(\boldsymbol{X}_a,\boldsymbol{X}_p,\boldsymbol{\delta},t)$ in circuits l of multi-circuit passive shield [13–15] and for passive contour screen geometric dimensions vector values $\boldsymbol{X}_p$ magnetic field induction vector $\boldsymbol{B}_p(Q_i,\boldsymbol{X}_a,\boldsymbol{X}_p,\boldsymbol{\delta},t)$ created by all circuits l of multi-circuit passive shield calculated according to Bio-Savart law (6). This passive shield magnetic field induction vector $\boldsymbol{B}_p(Q_i,\boldsymbol{X}_a,\boldsymbol{X}_p,\boldsymbol{\delta},t)$, based on Faraday law directed opposite to original magnetic field generated by power line and only by windings of active part of hybrid active-passive shield.

With help of passive part of hybrid active-passive shield, resulting magnetic field that remains uncompensated after operation of only active part of hybrid active-passive screen shielded.

Definition of geometric forward magneto static problem for overhead power lines and compensating winding magnetic field. Let's consider three-dimensional quasi-static magnetic field model created by overhead power lines. Let us set power transmission line wires currents amplitudes $\boldsymbol{A}_i$ and phases $\boldsymbol{\varphi}_i$ of industrial frequency ω. Let us write expressions for power transmission line wires currents in complex form

$$\boldsymbol{I}_i(t)=\boldsymbol{A}_i\exp j\left(\omega t+\varphi_i\right). \quad (10)$$

Then initial magnetic field induction vector $\boldsymbol{B}_L(Q_i,\boldsymbol{\delta},t)$ calculated according to Biot-Savart law based on (6) in magnetic field induction vectors sum form created by all power line wires at shielding space point Q_i [9]

$$B_L\left(Q_i,\delta,t\right)=\sum B_l\left(Q_i,\delta,t\right). \quad (11)$$

Consider design magnetic field mathematical model created by compensation windings of hybrid shield active part. Let us set vector $\boldsymbol{X}_a$ of spatial location and geometric dimensions of compensation windings of hybrid shield active part, as well as compensation windings currents amplitude $\boldsymbol{A}_{ai}$ and phase $\boldsymbol{\varphi}_{ai}$ [29–33]. Let us write expressions for compensation windings wires currents in complex form

$$\boldsymbol{I}_{\boldsymbol{ai}}(t)=\boldsymbol{A}_{ai}\exp j\left(\omega t+\varphi_{ai}\right). \quad (12)$$

Then magnetic field induction vector $\boldsymbol{B}_a(Q_i,\boldsymbol{X}_a,t)$ created by all compensating windings wires of active part of hybrid shield $\boldsymbol{B}_{ai}(Q_i,\boldsymbol{X}_a,t)$ in shielding space point Q_i calculated based on (6), according to the Biot-Savart law [6]

$$\boldsymbol{B}_a\left(Q_i,\boldsymbol{X}_a,t\right)=\sum\boldsymbol{B}_{ai}\left(Q_i,\boldsymbol{X}_a,t\right). \quad (13)$$

Then resulting magnetic field induction vector $\boldsymbol{B}_{Ra}(Q_i,\boldsymbol{X}_a,\boldsymbol{\delta},t)$ created by all power line wires and all windings of hybrid shield active part calculated as sum

$$\boldsymbol{B}_{Ra}\left(Q_i,\boldsymbol{X}_a,\boldsymbol{\delta},t\right)=\boldsymbol{B}_L\left(Q_i,\boldsymbol{\delta},t\right)+\boldsymbol{B}_a\left(Q_i,\boldsymbol{X}_a,t\right). \quad (14)$$

Then resulting magnetic field induction vector $\boldsymbol{B}_R(Q_i,\boldsymbol{X}_a,\boldsymbol{X}_p,\boldsymbol{\delta},t)$ calculated as sum of magnetic field induction vector $\boldsymbol{B}_L(Q_i,\boldsymbol{\delta},t)$ created by all power line wires, magnetic field induction vector $\boldsymbol{B}_a(Q_i,\boldsymbol{X}_a,t)$ created by all compensating windings of the of the hybrid shield active part, and magnetic field induction vector $\boldsymbol{B}_p(Q_i,\boldsymbol{X}_a,\boldsymbol{X}_p,\boldsymbol{\delta},t)$ created by all contours of passive part of hybrid shield in shielding space point Q_i

$$\boldsymbol{B}_R\left(Q_i,\boldsymbol{X}_a,\boldsymbol{X}_p,\boldsymbol{\delta},t\right)=\boldsymbol{B}_L\left(Q_i,\boldsymbol{\delta},t\right)+\ldots \\ \ldots+\boldsymbol{B}_a\left(Q_i,\boldsymbol{X}_a,t\right)+\boldsymbol{B}_p\left(Q_i,\boldsymbol{X}_a,\boldsymbol{X}_p,\boldsymbol{\delta},t\right). \quad (15)$$

Definition of geometric inverse magneto static problem for magnetic field combined electromagnetic shielding system synthesis. Hybrid active-passive shielding using multi-circuit windings of passive shield and compensating windings of active shield, created compensating magnetic field directed against original magnetic field created by power line. Hybrid active-passive shielding system synthesis task is to calculate spatial location coordinates of passive shield multi-circuit windings and active shield compensating windings as well as compensating windings currents magnitudes and phases. When hybrid active-passive shielding system designing, first of all, we will design a software controller in of an open-loop form [30–33] coarse control based on quasi-static magnetic field mathematical model [6, 7]. Then we will synthesis stabilizing precision controller in closed-loop form control [34–40], based on closed-loop system dynamics equations, taking into account models of actuators and measuring devices, disturbances and measurement noise, and designed to improve control accuracy compared to open-loop control based on quasi-static magnetic field mathematical model.

Let us introduce required parameters vector $\boldsymbol{X}$ for design problem of hybrid system of active-passive shielding, the components of which are vector $\boldsymbol{X}_a$ compensation windings geometric dimensions values, as well as compensation windings currents amplitudes $\boldsymbol{A}_{\omega i}$ and phases $\boldsymbol{\varphi}_{\omega i}$ of active part of hybrid active-passive shielding system, as well as vector $\boldsymbol{X}_p$ of geometric dimensions, thickness and material of the shield of passive part of hybrid active-passive shielding system. Then, for given initial required parameters vector values $\boldsymbol{X}$ and for uncertainty parameters vector $\boldsymbol{\delta}$ of hybrid active-passive shielding system resulting magnetic field induction vector effective value $\boldsymbol{B}_R(\boldsymbol{X},\boldsymbol{\delta},P_i)$ in shielding space point Q_i calculated by COMSOL Multiphysics software environment using the of the of the resulting magnetic field instantaneous induction value vector $\boldsymbol{B}_R(Q_i,\boldsymbol{X}_a,\boldsymbol{X}_p,\boldsymbol{\delta},t)$ from (15).

In [16–18] magnetic field shielding system synthesis problem reduced to one scalar criterion optimizing problem, which calculated as linear convolution of induction values in shielding space different points. However, calculating problem correctly of weighting factors with help of which scalar optimization criterion formed in general form is an ill-posed problem and its solution requires special approaches [26–30]. In addition, in formulation of magnetic field shielding system designing problem uncertainties of initial magnetic field models and of control system parameters were not taken into account at all. Therefore, in contrast to works [16–18] robust hybrid active-passive shielding system synthesis problem reduced to vector game solution calculating [41]

$$\boldsymbol{B}_R(\boldsymbol{X},\boldsymbol{\delta})=\langle\boldsymbol{B}_R(\boldsymbol{X},\boldsymbol{\delta},Q_i)\rangle. \quad (16)$$

In this vector game, it is necessary to find minimum of game payoff vector (16) from required parameters vector $\boldsymbol{X}$ for hybrid active-passive shielding system synthesis problem, but maximum of same game payoff vector (16) from uncertainty parameters vector $\boldsymbol{\delta}$ for hybrid active-passive shielding system

Components of vector game payoff (17) are resulting magnetic field induction effective values $\boldsymbol{B}_R(\boldsymbol{X},\boldsymbol{\delta},Q_i)$ at all of the shielding space considered points Q_i.

Components of the vector game payoff (16) are nonlinear functions of required parameters vector $\boldsymbol{X}$ and of uncertainty parameters vector $\boldsymbol{\delta}$ of of a hybrid active-passive

shielding system synthesis problem [19] and calculated by COMSOL Multiphysics software environment.

Vector game solution algorithm. Let's consider algorithm for vector game solution (16) calculating. The works [41] consider various approaches to computing by vector games solutions based on various heuristic approaches. Unlike works [31, 32], in this work, in order to find unique solution of vector game from set of Pareto-optimal solutions, in addition to the vector payoff (16) also used information about binary relationships of local solutions preferences relative to each other.

A feature of solution calculated problem under consideration is vector payoff (16) multi-extremal nature, so that possible solutions considered region contains local minima and maxima. This is due to fact that when resulting magnetic field induction level minimizing in shielding space one point, induction level in another point increases due to under compensation or overcompensation of the original magnetic field. Therefore, to calculate vector game solution under consideration, it is advisable stochastic multi-agent particle swarm optimization (PSO) algorithms used [41].

To calculate vector games solutions of stochastic multi-agent heuristic optimization methods used causes certain difficulties, however, this direction continues to develop intensively using various heuristic techniques. For calculating original vector game solution (16) stochastic multi-agent PSO algorithm used based on set of particle swarms, number of which equal to number of components of vector game payoff (16).

When calculating one single global solution to vector game (16) of scalar games solutions that are components of game vector (16) calculated using individual swarms. To calculate one single global solution to the vector game (16) individual swarms exchange information with each other during local games optimal solutions calculation. In contrast to works [36–38], at each swarm particle movement step binary preference functions of local solution obtained by one particle of swarm and global solution obtained by all swarms used [41]. This approach allows calculated solution that minimizes maximum resulting magnetic field induction level value for all considered shielding space points.

PSO is a robust stochastic optimization method based on the motion and intelligence of swarms. In PSO, each individual is treated as a particle in the design space with position and velocity vectors that fly through the problem space following the current optimal particles. PSO is a population-based search algorithm. The advantages of PSO are that it is simple to implement and has few configurable parameters. PSO is initialized with a population of n random particles (solutions), which then searches for optima by updating generations. At each iteration, each particle is updated with the «best» solution (fitness) it has achieved so far, which is called «best». The other «best» solution, which is the global best solution achieved so far by any particle in the population, is called «gbest» [41].

The PSO algorithm is a gradient-free algorithm. The algorithm does not require the calculation of the gradient or the Hessian matrix of second derivatives. The PSO algorithm is actually an optimization algorithm based on random search. A significant advantage of the PSO algorithm is the ability to calculate the global extremum due to the exchange of information between individual particles during the search for local extrema using individual particles. In fact, the «particle swarm» is a widely used approach for searching for a global extremum with a multi-start.

However, the main disadvantage of the PSO algorithm compared to deterministic optimization methods based on gradient methods is the relatively long computation time. This is, firstly, due to the search for one optimum using a swarm of particles, which increases the search time by approximately a number of times equal to the number of particles in the swarm. The search time especially increases when solving a vector optimization problem using multiple swarms of particles, the number of swarms is equal to the number of components of the vector objective function. Naturally, each component of the objective function calculated using a swarm of particles.

Therefore, to speed up the calculation of the global optimum, it is advisable to use the PSO algorithm for a «rough» calculation of the position of the global optimum. It is advisable to calculate the refined position of the global optimum using deterministic algorithms based on gradient optimization methods, and possibly using the matrix of second derivatives – the Hessian matrix.

The expediency of such an approach is also due to the fact, that in the region of the extremum, the components of the gradient vector of the objective function tend to zero. And although the PSO algorithm is formally a gradient-free optimization method and does not require calculating the gradient of the objective function, the speeds of particle movement in the PSO algorithm, which are determined based on a random search, actually play the role of the gradient components of the objective function. Naturally, in the region of the extremum, these speeds of particle movement, calculated based on a random search, also tend to zero, which determines the use of optimization algorithms based on the second derivatives – the Hessian matrix.

Sequential Quadratic Programming (SQP) is one of the most successful methods for solving smooth nonlinear optimization problems with constraints. The two most significant features of this algorithm are the speed of convergence and accuracy. SQP finds the search direction using linear approximation of the constraints and quadratic approximation of the design objective functions.

Let us consider the application of SQP method to solve this problem. This method is a combination of the Gauss-Newton method with determination of the direction of motion using the quasi-Newton algorithm. SQP is one of the most successful methods for solving smooth nonlinear constrained optimization problems. The two most significant features of this algorithm are the speed of convergence and accuracy. SQP finds the search direction using a linear approximation of the constraints and a quadratic approximation of the design objective functions. The solution procedure is based on formulating and solving a quadratic subproblem in each iteration.

Let us first consider the minimization of the quadratic norm of L2, commonly called the unconstrained least squares problem

$$f(x)=\frac{1}{2}\sum_{i=1}^{l} f_i(x)^2 \ . \tag{17}$$

The gradient of this objective function can be represented as follows

$$\nabla f(x)=\nabla F(x)F(x), \tag{18}$$

where $\nabla F(x)=(\nabla f_1(x),...,\nabla f_l(x))$ is the Jacobian of this function and it is assumed that the components of the objective function can be differentiated twice. Then the matrix of second derivatives of the objective function – the Hesse matrix can be written as follows

$$\nabla^2 f(x) = \nabla F(x) \nabla F(x)^T + B(x), \quad (19)$$

where

$$B(x) = \sum_{i=1}^{l} f_i(x) \nabla^2 f_i(x) \nabla^2 f_i(x). \quad (20)$$

Then the iterative procedure for choosing the direction d_k of movement using Newton's method can be reduced to solving the linear system

$$\nabla^2 f(x_k) d + \nabla f(x_k) = 0. \quad (21)$$

For the iterative finding of the vector of the sought parameters

$$x_{k+1} = x_k + \alpha_k d_k \quad (22)$$

where a recurrent equation d_k can be obtained in which is the solution to the optimization problem, and α_k is the experimentally determined parameter.

This algorithm uses the Gauss–Newton method, which is a traditional algorithm for solving the problem of the nonlinear least squares method, to calculate the direction d_k of motion (22). In general, the Gauss–Newton method allows you to obtain a solution to the problem of sequential quadratic programming using only first-order derivatives, but in real situations it often cannot obtain a solution. Therefore, to improve convergence, second-order methods are used, which use the matrix of second derivatives of the objective function – the Jacobian matrix when solving optimization problems without constraints. Second-order algorithms, compared with first-order methods, allow you to effectively obtain a solution in a region close to the optimal point, when the components of the gradient vector have sufficiently small values.

The main problem of applying the SQP method is the need to use special methods to ensure negative eigenvalues when approximating the Hessian matrix in the case of alternative approaches. Currently, the Levenberg-Marquardt algorithm is used for pseudo-inversion of the Hessian matrix (21).

Minimax problems are widely used in robust control. If it is necessary to find the minimum for some variables and the maximum for other variables of the same objective function, then a necessary condition for the optimality of this minimax problem is that the gradient of the objective function is equal to zero for all variables, regardless of whether the objective function is minimized or maximized. When solving this minimax problem numerically, to find the direction of movement, it is necessary to use the components of the gradient of the objective function for those variables for which maximization is performed, and it is necessary to use the components of the antigradient (i.e., the gradient taken with the opposite sign) for those variables for which minimization is performed.

Numerical solution of nonlinear programming problem (17) with constraints, with the exception of direct methods, involves the use of partial derivatives. Analytical expressions for derivatives (18) in the problems under consideration are usually impossible to obtain; therefore, derivatives are calculated using various schemes – a two-way scheme, a forward scheme, or a backward scheme, which are approximate numerical calculations of derivatives using difference schemes.

Simulation results. Unlike works [13–18], in this work spatial location coordinates of contours for multi-circuit passive screen calculated as multi-criteria zero-sum game (16) solution for initial magnetic field electromagnetic hybrid active-passive shielded. In process combined active and multi-loop passive shielding system synthesis spatial location coordinates of 16 conductors for multi-circuit passive shield calculated. In addition, spatial location coordinates of two compensation windings, as well as currents and phases in these windings of active shielding system also calculated.

Let us consider combined shield operation to magnetic field reduced in residential building located near power lines with wires triangular arrangement. Figure 3 shows initial magnetic field induction distribution generated by power line with wires triangular arrangement.

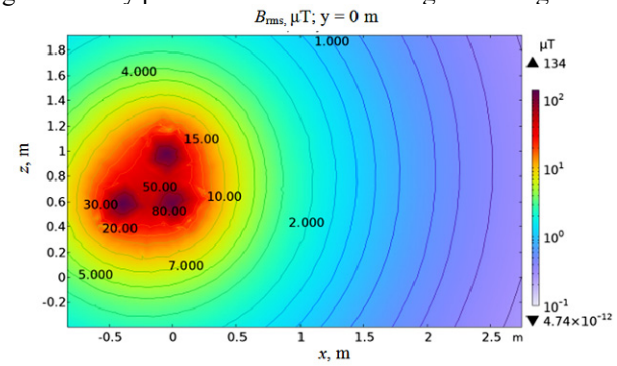

Fig. 3. Initial magnetic field induction distribution

As can seen from Fig. 3, initial magnetic field induction level in shielding space is more than 4 times higher than sanitary standards for population safe living of 0.5 μT.

Figure 4 shows resulting magnetic field induction distribution when a multi-circuit passive shield operating only. As can see from Figure 4, resulting magnetic field induction level decreased by approximately 1.3 times, but exceeds sanitary standards by approximately 3 times.

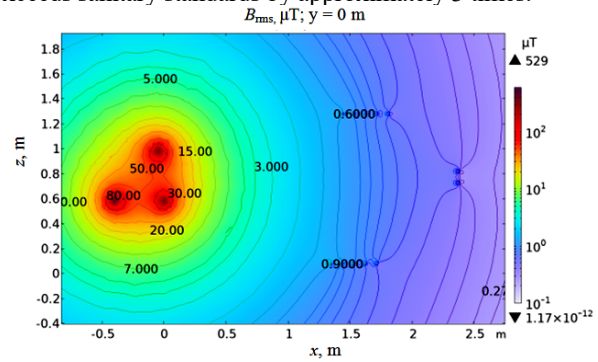

Fig. 4. Resulting magnetic field when multi-circuit passive shield operating only

Figure 5 shows the of the resulting magnetic field induction distribution when active shield with two compensating windings operating only. As can seen from Fig. 5, resulting magnetic field induction level decreased by approximately 8 times.

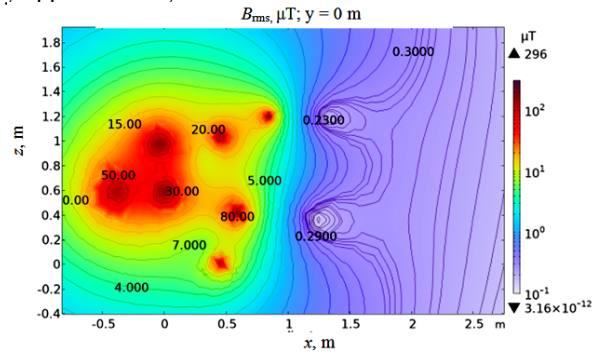

Fig. 5. Resulting magnetic field when active shielding system with two windings operating only

Figure 6 shows resulting magnetic field induction distribution during hybrid shield operation. As can seen from Fig. 6, resulting magnetic field induction level decreased by approximately 8.3 times. At the same time, resulting magnetic field induction level in shielding space does not exceed 0.24 μT, which is more than two times less than induction level of industrial frequency magnetic field for population safe living.

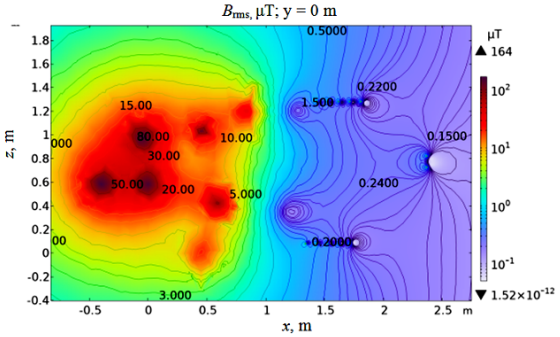

Fig. 6. Resulting field when hybrid shield working

Moreover, in comparison with active shield operation only, when combined shield operating, initial magnetic field shielding effective occurs in significantly larger shielding space.

Let us now consider resulting magnetic field induction distribution level along shielding space length based on three-dimensional magnetic field modeling.

First, let's consider resulting magnetic field three-dimensional modeling results when multi-circuit passive shield operating only. Figure 7 shows the of magnetic field induction distribution along passive shield length for various coordinates along multi-circuit passive shield height and width.

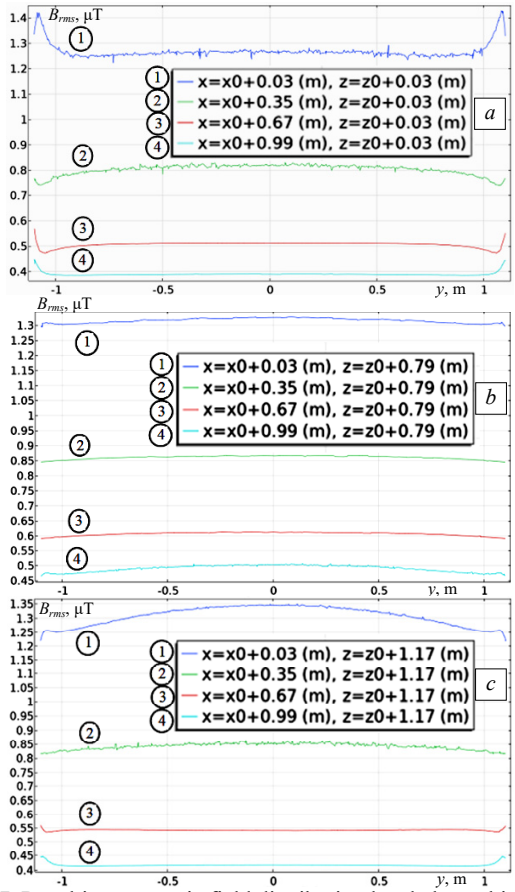

Fig. 7. Resulting magnetic field distribution level along shielding space length when multi-circuit passive shield operating only

As can seen from Fig. 7, shielding efficiency when multi-circuit passive shield using only remains almost constant along shield length and only slightly decreases at shielding area edges.

Let us now consider three-dimensional modeling results of resulting magnetic field when active shield operating only. Figure 8 shows resulting magnetic field induction distribution along length for various coordinates along shielding space height and width.

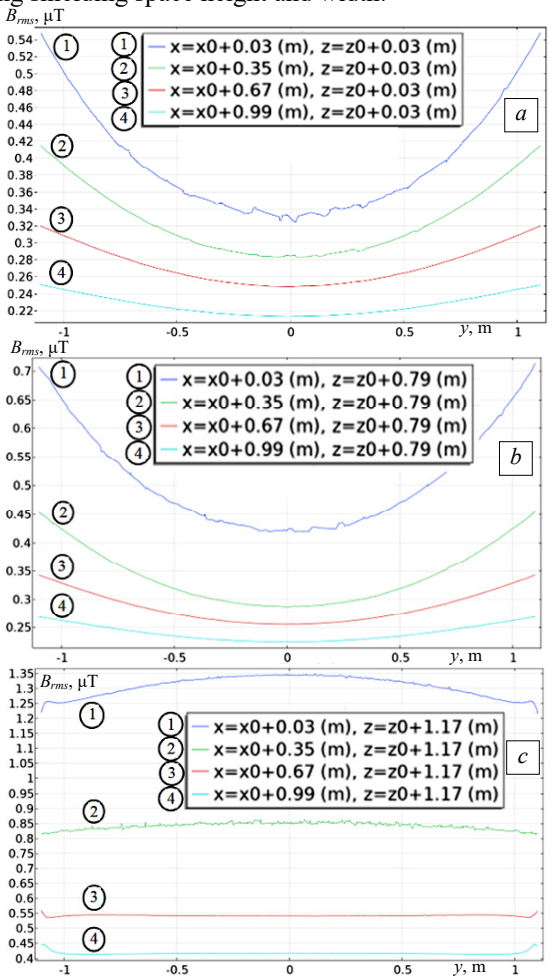

Fig. 8. Resulting magnetic field level distribution along shielding space length when active shield operating only

As can seen from Fig. 8, when active shield operating only in central part along shielding space length, resulting magnetic field induction level is in range 0.22–0.42 μT. However, at shielding region edges, resulting magnetic field induction level increases by approximately 1.3–1.5 times to values of 0.27–0.7 μT.

Let us now consider three-dimensional modeling results of resulting magnetic field during combined screen operation. Figure 9 shows resulting magnetic field induction distribution along length for various coordinates along shielding space height and width when combined shield operating.

As can seen from Fig. 9, when combined shield operates in central part along shielding space length, resulting magnetic field induction level slightly reduced compared to induction level when active screen operating only. In addition, at shielding area edges, resulting magnetic field induction level increases slightly less compared to induction level when active shield operating only. Thus, with the help of combined shield, resulting magnetic field induction level reduced in significantly larger space compared to active shield operation only.

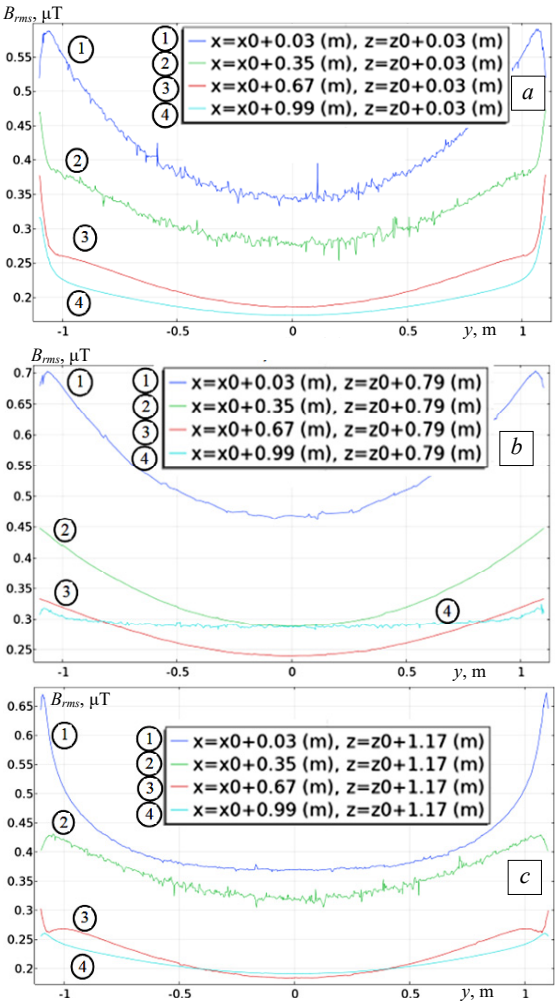

Fig. 9. Resulting magnetic field distribution level along shielding space length during combined screen operation

Combined hybrid active and multi-loop passive shielding system experimental setup description. To conduct experimental studies combined shield experimental setup developed. All experimental studies carried out on the magnetodynamic measuring stand at the Anatolii Pidhornyi Institute of Power Machines and Systems of the National Academy of Sciences of Ukraine [42].

Fig. 10. Multi-circuit passive shield

Experimental setup contains single-circuit power line setup with «Triangle» type wires arrangement, two compensation windings of active shielding system and a multi-circuit electromagnetic shield made of aluminum rod with 8 mm diameter. Figure 10 shows an experimental installation of such multi-circuit passive shield. Two magnetic field sensors installed inside passive shield.

As Fig. 11 shows, to implement two closed-loop control loops for two compensation windings of active shielding system with feedback on resulting magnetic field.

During control loops adjusting process, these sensors axes seted in such way as to maximum magnetic field induction value measured generated by compensation winding of corresponding compensating channel. This magnetic field sensors axes installation makes it possible to minimize channels on each other influence when they work together.

Fig. 11. Magnetometer installation diagram

Fig. 12. Two compensating windings of active shielding system

Two more magnetic field sensors installed inside passive shield, which axes directed parallel to coordinate axes. These two sensors used in system for resulting magnetic field space-time characteristics measuring. This measuring system used to control loops adjust of active shielding system of combined magnetic field shielding.

Figure 12 shows two compensation windings of active shielding system.

Figure 13 shows combined shielding control system. To measure resulting magnetic field inside shielding space a three-coordinate magnetometer type «TES 1394S triaxial ELF magnetic field meter» is used.

Fig. 13. Combined shielding control system

Experimental studies results. Let us consider experimental studies results of resulting magnetic field distribution dependences with combined multi-circuit electromagnetic shield consisting of two compensation windings of active shield and multi-circuit passive shield consisting of 16 circuits.

Let us now consider of experimentally measured distribution level of resulting magnetic field induction along shielding space length based on three-dimensional modeling of magnetic field distribution.

First, let us consider the experimentally measured results of resulting magnetic field when multi-circuit passive shield operating only. Figure 14 shows experimentally measured distributions of magnetic field induction along passive shield length for various coordinates along multi-circuit passive shield height and width.

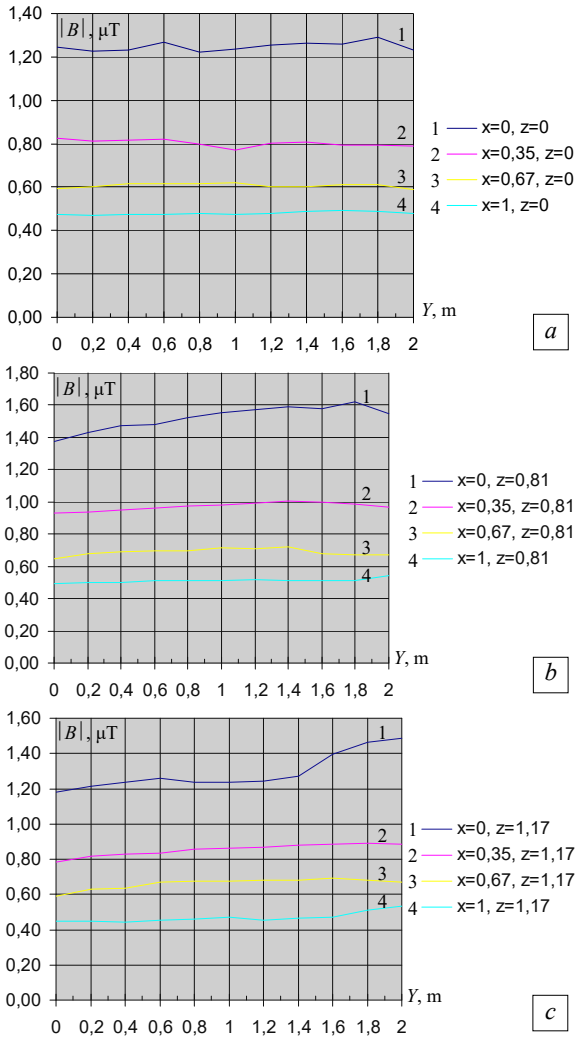

Fig. 14. Experimentally measured distributions of resulting magnetic field level along shielding space length when multi-circuit passive shield operating only

As can seen from Fig. 14, shielding efficiency when multi-circuit passive shield using only remains almost constant along shielding space length and only slightly decreases along shielding area edges, which corresponds to calculated magnetic field distributions shown in Fig. 6.

Let us now consider experimentally measured values results of resulting magnetic field when active shield operating only. Figure 15 shows experimentally measured distributions of resulting magnetic field induction along length for various coordinates along shielding space height and width.

As can seen from Fig. 15, when active shield operating only in central part along shielding space length, experimentally measured levels values of resulting magnetic field induction distribution coincide with calculated magnetic field distributions shown in Fig. 8 with 20 % accuracy.

Let us now consider experimentally measured distributions of resulting magnetic field during operation of combined active and multi-loop passive shielding system. Figure 16 shows experimentally measured distributions of resulting magnetic field induction along length for various coordinates along shielding space height and width during of the combined shield operation.

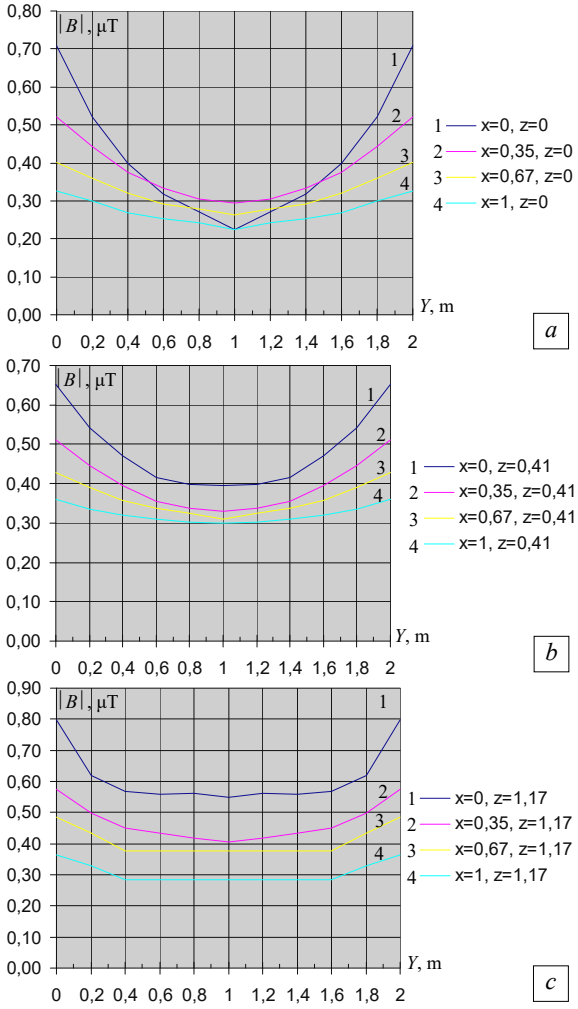

Fig. 15. Experimentally measured distributions of resulting magnetic field level along shielding space length when active shield operating only

As can seen from Fig. 16, when combined shield operating, the experimentally measured induction levels values of resulting magnetic field distribution coincide with calculated magnetic field distributions shown in Fig. 9 with 20 % accuracy.

Thus, based on three-dimensional modeling results and experimental studies, it has been established that with combined shield help resulting magnetic field induction level reduced in significantly larger space compared to active screen operation only.

Conclusions.

1. For the first time system synthesis methodology for robust combined active and multi-circuit passive shielding system to improve effectiveness of of industrial frequency magnetic field reduction in residential buildings space created by overhead power lines wires developed.

2. Developed system synthesis methodology for robust combined electromagnetic active and multi-circuit passive shielding system synthesis based on vector game solution. Vector game payoff calculated by finite element calculations system COMSOL Muliphysics. Vector game solution calculated based on hybrid optimization algorithm, which globally explores synthesis search space using particle swarm optimization and gradient-based sequential quadratic programming to rapidly calculated optimum synthesis point from Pareto optimal solutions taking into account binary preferences relationships used.

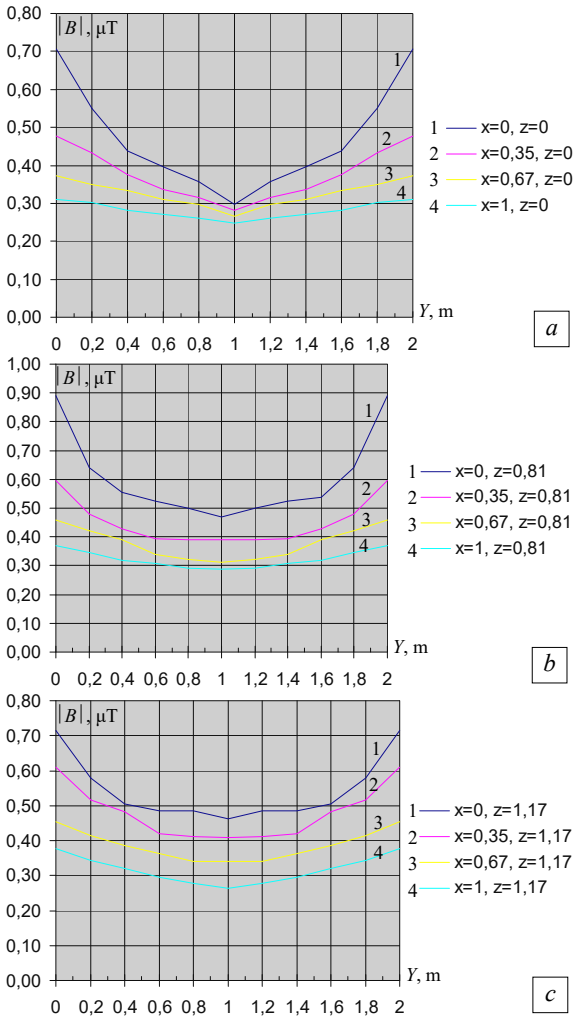

Fig. 16. Experimentally measured distributions along of shielding space length of resulting magnetic field level during of the combined shield operation

3. Performed theoretical studies results shown that shielding factor by only electromagnetic multi-circuit passive shield made from 1.5 mm thickness solid aluminum plate is about 2 units, only active shield made from winding form consisting of 20 turns is about 4 units. When combined electromagnetic passive and active shield used, shielding factor was more 10 units, which confirms its high efficiency, exceeding product shielding factors of passive and active shields.

4. Performed experimental studies results confirmed modeling and theoretical studies results. Experimentally measured induction levels values of resulting magnetic field distribution coincide with calculated magnetic field distributions with 20 % accuracy.

5. Practical used of developed combined active and multi-loop passive shielding system will allow magnetic field level reducing in residential building from phase wires triangular arrangement of overhead power lines to population safe level of 0.5 μT.

6. In the future, it is necessary to implement such combined electromagnetic active and multi-circuit passive shielding systems to normalize the field in real residential building.

Conflict of interest. The authors declare that they have no conflicts of interest.

REFERENCES

1. Sung H., Ferlay J., Siegel R.L., Laversanne M., Soerjomataram I., Jemal A., Bray F. Global Cancer Statistics 2020: GLOBOCAN Estimates of Incidence and Mortality Worldwide for 36 Cancers in 185 Countries. *CA: A Cancer Journal for Clinicians*, 2021, vol. 71, no. 3, pp. 209-249. doi: https://doi.org/10.3322/caac.21660.

2. *Directive 2013/35/EU of the European Parliament and of the Council of 26 June 2013 on the minimum health and safety requirements regarding the exposure of workers to the risks arising from physical agents (electromagnetic fields)*. Available at: http://data.europa.eu/eli/dir/2013/35/oj (Accessed 20 February 2025).

3. *The International EMF Project. Radiation & Environmental Health Protection of the Human Environment World Health Organization*. Geneva, Switzerland, 1996. 2 p. Available at: https://www.who.int/initiatives/the-international-emf-project (Accessed 20 February 2025).

4. Rozov V., Grinchenko V., Tkachenko O., Yerisov A. Analytical Calculation of Magnetic Field Shielding Factor for Cable Line with Two-Point Bonded Shields. *2018 IEEE 17th International Conference on Mathematical Methods in Electromagnetic Theory (MMET)*, 2018, pp. 358-361. doi: https://doi.org/10.1109/MMET.2018.8460425.

5. Rozov V.Y., Zavalnyi A.V., Zolotov S.M., Gretskikh S.V. The normalization methods of the static geomagnetic field inside houses. *Electrical Engineering & Electromechanics*, 2015, no. 2, pp. 35-40. doi: https://doi.org/10.20998/2074-272X.2015.2.07.

6. Rozov V.Y., Pelevin D.Y., Kundius K.D. Simulation of the magnetic field in residential buildings with built-in substations based on a two-phase multi-dipole model of a three-phase current conductor. *Electrical Engineering & Electromechanics*, 2023, no. 5, pp. 87-93. doi: https://doi.org/10.20998/2074-272X.2023.5.13.

7. Rozov V.Yu., Reutskyi S.Yu., Pelevin D.Ye., Kundius K.D. Approximate method for calculating the magnetic field of 330-750 kV high-voltage power line in maintenance area under voltage. *Electrical Engineering & Electromechanics*, 2022, no. 5, pp. 71-77. doi: https://doi.org/10.20998/2074-272X.2022.5.12.

8. Salceanu A., Paulet M., Alistar B.D., Asiminicesei O. Upon the contribution of image currents on the magnetic fields generated by overhead power lines. *2019 International Conference on Electromechanical and Energy Systems (SIELMEN)*. 2019. doi: https://doi.org/10.1109/sielmen.2019.8905880.

9. Del Pino Lopez J.C., Romero P.C. Influence of different types of magnetic shields on the thermal behavior and ampacity of underground power cables. *IEEE Transactions on Power Delivery*, Oct. 2011, vol. 26, no. 4, pp. 2659-2667. doi: https://doi.org/10.1109/tpwrd.2011.2158593.

10. Hasan G.T., Mutlaq A.H., Ali K.J. The Influence of the Mixed Electric Line Poles on the Distribution of Magnetic Field. *Indonesian Journal of Electrical Engineering and Informatics (IJEEI)*, 2022, vol. 10, no. 2, pp. 292-301. doi: https://doi.org/10.52549/ijeei.v10i2.3572.

11. Victoria Mary S., Pugazhendhi Sugumaran C. Investigation on magneto-thermal-structural coupled field effect of nano coated 230 kV busbar. *Physica Scripta*, 2020, vol. 95, no. 4, art. no. 045703. doi: https://doi.org/10.1088/1402-4896/ab6524.

12. Ippolito L., Siano P. Using multi-objective optimal power flow for reducing magnetic fields from power lines. *Electric Power Systems Research*, 2004, vol. 68, no. 2, pp. 93-101. doi: https://doi.org/10.1016/S0378-7796(03)00151-2.

13. Barsali S., Giglioli R., Poli D. Active shielding of overhead line magnetic field: Design and applications. *Electric Power Systems Research*, May 2014, vol. 110, pp. 55-63. doi: https://doi.org/10.1016/j.epsr.2014.01.005.

14. Bavastro D., Canova A., Freschi F., Giaccone L., Manca M. Magnetic field mitigation at power frequency: design principles and case studies. *IEEE Transactions on Industry Applications*, May 2015, vol. 51, no. 3, pp. 2009-2016. doi: https://doi.org/10.1109/tia.2014.2369813.

15. Beltran H., Fuster V., García M. Magnetic field reduction screening system for a magnetic field source used in industrial applications. *9 Congreso Hispano Luso de Ingeniería Eléctrica (9 CHLIE)*, Marbella (Málaga, Spain), 2005, pp. 84-99.

16. Bravo-Rodríguez J., Del-Pino-López J., Cruz-Romero P. A Survey on Optimization Techniques Applied to Magnetic Field Mitigation in Power Systems. *Energies*, 2019, vol. 12, no. 7, art. no. 1332. doi: https://doi.org/10.3390/en12071332.

17. Canova A., del-Pino-López J.C., Giaccone L., Manca M. Active Shielding System for ELF Magnetic Fields. *IEEE Transactions on Magnetics*, March 2015, vol. 51, no. 3, pp. 1-4. doi: https://doi.org/10.1109/tmag.2014.2354515.

18. Canova A., Giaccone L. Real-time optimization of active loops for the magnetic field minimization. *International Journal of Applied Electromagnetics and Mechanics*, Feb. 2018, vol. 56, pp. 97-106. doi: https://doi.org/10.3233/jae-172286.
19. Canova A., Giaccone L., Cirimele V. Active and passive shield for aerial power lines. *Proc. of the 25th International Conference on Electricity Distribution (CIRED 2019)*, 3-6 June 2019, Madrid, Spain. Paper no. 1096.
20. Grinchenko V.S. Mitigation of three-phase power line magnetic field by grid electromagnetic shield. *Technical Electrodynamics*, 2018, no. 4, pp. 29-32. (Ukr). doi: https://doi.org/10.15407/techned2018.04.029.
21. Celozzi S. Active compensation and partial shields for the power-frequency magnetic field reduction. *2002 IEEE International Symposium on Electromagnetic Compatibility*, Minneapolis, MN, USA, 2002, vol. 1, pp. 222-226. doi: https://doi.org/10.1109/isemc.2002.1032478.
22. Celozzi S., Garzia F. Active shielding for power-frequency magnetic field reduction using genetic algorithms optimization. *IEE Proceedings - Science, Measurement and Technology*, 2004, vol. 151, no. 1, pp. 2-7. doi: https://doi.org/10.1049/ip-smt:20040002.
23. Celozzi S., Garzia F. Magnetic field reduction by means of active shielding techniques. *WIT Transactions on Biomedicine and Health*, 2003, vol. 7, pp. 79-89. doi: https://doi.org/10.2495/ehr030091.
24. Martynenko G. Analytical Method of the Analysis of Electromagnetic Circuits of Active Magnetic Bearings for Searching Energy and Forces Taking into Account Control Law. *2020 IEEE KhPI Week on Advanced Technology (KhPIWeek)*, 2020, pp. 86-91. doi: https://doi.org/10.1109/KhPIWeek51551.2020.9250138.
25. Popov A., Tserne E., Volosyuk V., Zhyla S., Pavlikov V., Ruzhentsev N., Dergachov K., Havrylenko O., Shmatko O., Averyanova Y., Ostroumov I., Kuzmenko N., Sushchenko O., Zaliskyi M., Solomentsev O., Kuznetsov B., Nikitina T. Invariant Polarization Signatures for Recognition of Hydrometeors by Airborne Weather Radars. *Computational Science and Its Applications – ICCSA 2023. Lecture Notes in Computer Science*, 2023, vol. 13956, pp. 201-217. doi: https://doi.org/10.1007/978-3-031-36805-9_14.
26. Sushchenko O., Averyanova Y., Ostroumov I., Kuzmenko N., Zaliskyi M., Solomentsev O., Kuznetsov B., Nikitina T., Havrylenko O., Popov A., Volosyuk V., Shmatko O., Ruzhentsev N., Zhyla S., Pavlikov V., Dergachov K., Tserne E. Algorithms for Design of Robust Stabilization Systems. *Computational Science and Its Applications – ICCSA 2022. ICCSA 2022. Lecture Notes in Computer Science*, 2022, vol. 13375, pp. 198-213. doi: https://doi.org/10.1007/978-3-031-10522-7_15.
27. Ostroverkhov M., Chumack V., Monakhov E., Ponomarev A. Hybrid Excited Synchronous Generator for Microhydropower Unit. *2019 IEEE 6th International Conference on Energy Smart Systems (ESS)*, Kyiv, Ukraine, 2019, pp. 219-222. doi: https://doi.org/10.1109/ess.2019.8764202.
28. Ostroverkhov M., Chumack V., Monakhov E. Ouput Voltage Stabilization Process Simulation in Generator with Hybrid Excitation at Variable Drive Speed. *2019 IEEE 2nd Ukraine Conference on Electrical and Computer Engineering (UKRCON)*, Lviv, Ukraine, 2019, pp. 310-313. doi: https://doi.org/10.1109/ukrcon.2019.8879781.
29. Tytiuk V., Chornyi O., Baranovskaya M., Serhiienko S., Zachepa I., Tsvirkun L., Kuznetsov V., Tryputen N. Synthesis of a fractional-order $PI^{\lambda}D^{\mu}$-controller for a closed system of switched reluctance motor control. *Eastern-European Journal of Enterprise Technologies*, 2019, no. 2 (98), pp. 35-42. doi: https://doi.org/10.15587/1729-4061.2019.160946.
30. Shchur I., Turkovskyi V. Comparative Study of Brushless DC Motor Drives with Different Configurations of Modular Multilevel Cascaded Converters. *2020 IEEE 15th International Conference on Advanced Trends in Radioelectronics, Telecommunications and Computer Engineering (TCSET)*, Lviv-Slavske, Ukraine, 2020, pp. 447-451. doi: https://doi.org/10.1109/tcset49122.2020.235473.
31. Volosyuk V., Zhyla S., Pavlikov V., Ruzhentsev N., Tserne E., Popov A., Shmatko O., Dergachov K., Havrylenko O., Ostroumov I., Kuzmenko N., Sushchenko O., Averyanova Yu., Zaliskyi M., Solomentsev O., Kuznetsov B., Nikitina T. Optimal Method for Polarization Selection of Stationary Objects Against the Background of the Earth's Surface. *International Journal of Electronics and Telecommunications*, 2022, vol. 68, no. 1, pp. 83-89. doi: https://doi.org/10.24425/ijet.2022.139852.
32. Halchenko V., Trembovetska R., Bazilo C., Tychkova N. Computer Simulation of the Process of Profiles Measuring of Objects Electrophysical Parameters by Surface Eddy Current Probes. *Lecture Notes on Data Engineering and Communications Technologies*, 2023, vol. 178, pp. 411-424. doi: https://doi.org/10.1007/978-3-031-35467-0_25.
33. Halchenko V., Bacherikov D., Filimonov S., Filimonova N. Improvement of a Linear Screw Piezo Motor Design for Use in Accurate Liquid Dosing Assembly. *Smart Technologies in Urban Engineering. STUE 2022. Lecture Notes in Networks and Systems*, 2023, vol. 536, pp. 237-247. doi: https://doi.org/10.1007/978-3-031-20141-7_22.
34. Maksymenko-Sheiko K.V., Sheiko T.I., Lisin D.O., Petrenko N.D. Mathematical and Computer Modeling of the Forms of Multi-Zone Fuel Elements with Plates. *Journal of Mechanical Engineering*, 2022, vol. 25, no. 4, pp. 32-38. doi: https://doi.org/10.15407/pmach2022.04.032.
35. Hontarovskyi P.P., Smetankina N.V., Ugrimov S.V., Garmash N.H., Melezhyk I.I. Computational Studies of the Thermal Stress State of Multilayer Glazing with Electric Heating. *Journal of Mechanical Engineering*, 2022, vol. 25, no. 1, pp. 14-21. doi: https://doi.org/10.15407/pmach2022.02.014.
36. Kostikov A.O., Zevin L.I., Krol H.H., Vorontsova A.L. The Optimal Correcting the Power Value of a Nuclear Power Plant Power Unit Reactor in the Event of Equipment Failures. *Journal of Mechanical Engineering*, 2022, vol. 25, no. 3, pp. 40-45. doi: https://doi.org/10.15407/pmach2022.03.040.
37. Rusanov A.V., Subotin V.H., Khoryev O.M., Bykov Y.A., Korotaiev P.O., Ahibalov Y.S. Effect of 3D Shape of Pump-Turbine Runner Blade on Flow Characteristics in Turbine Mode. *Journal of Mechanical Engineering*, 2022, vol. 25, no. 4, pp. 6-14. doi: https://doi.org/10.15407/pmach2022.04.006.
38. Kurennov S., Smetankina N., Pavlikov V., Dvoretskaya D., Radchenko V. Mathematical Model of the Stress State of the Antenna Radome Joint with the Load-Bearing Edging of the Skin Cutout. *Lecture Notes in Networks and Systems*, 2022, vol. 305, pp. 287-295. doi: https://doi.org/10.1007/978-3-030-83368-8_28.
39. Kurennov S., Smetankina N. Stress-Strain State of a Double Lap Joint of Circular Form. Axisymmetric Model. *Lecture Notes in Networks and Systems*, 2022, vol 367 LNNS, pp. 36-46. doi: https://doi.org/10.1007/978-3-030-94259-5_4.
40. Smetankina N., Merkulova A., Merkulov D., Misiura S., Misiura I. Modelling Thermal Stresses in Laminated Aircraft Elements of a Complex Form with Account of Heat Sources. *Lecture Notes in Networks and Systems*, 2023, vol. 534 LNNS, pp. 233-246. doi: https://doi.org/10.1007/978-3-031-15944-2_22.
41. Hashim F.A., Hussain K., Houssein E.H., Mabrouk M.S., Al-Atabany W. Archimedes optimization algorithm: a new metaheuristic algorithm for solving optimization problems. *Applied Intelligence*, 2021, vol. 51, no. 3, pp. 1531-1551. doi: https://doi.org/10.1007/s10489-020-01893-z.
42. Baranov M.I., Rozov V.Y., Sokol Y.I. To the 100th anniversary of the National Academy of Sciences of Ukraine – the cradle of domestic science and technology. *Electrical Engineering & Electromechanics*, 2018, no. 5, pp. 3-11. doi: https://doi.org/10.20998/2074-272X.2018.5.01.

Received 10.04.2025
Accepted 05.06.2025
Published 02.11.2025

B.I. Kuznetsov[1], *Doctor of Technical Science, Professor,*
T.B. Nikitina[2], *Doctor of Technical Science, Professor,*
I.V. Bovdui[1], *PhD, Senior Research Scientist,*
K.V. Chunikhin[1], *PhD, Senior Research Scientist,*
V.V. Kolomiets[2], *PhD, Assistant Professor,*
B.B. Kobylianskyi[2], *PhD, Assistant Professor,*
[1] Anatolii Pidhornyi Institute of Power Machines and Systems of the National Academy of Sciences of Ukraine,
2/10, Komunalnykiv Str., Kharkiv, 61046, Ukraine,
e-mail: kuznetsov.boris.i@gmail.com (Corresponding Author)
[2] Bakhmut Education Research and Professional Pedagogical Institute V.N. Karazin Kharkiv National University,
9a, Nosakov Str., Bakhmut, Donetsk Region, 84511, Ukraine.

How to cite this article:
Kuznetsov B.I., Nikitina T.B., Bovdui I.V., Chunikhin K.V., Kolomiets V.V., Kobylianskyi B.B. Synthesis of combined shielding system for overhead power lines magnetic field normalization in residential building space. *Electrical Engineering & Electromechanics*, 2025, no. 6, pp. 40-50. doi: https://doi.org/10.20998/2074-272X.2025.6.06